Magneto-optic study of the interface in semimagnetic semiconductor heterostructures: Intrinsic effect and interface profile in CdTe-$Cd_{1-x}Mn_xTe$

W. Grieshaber, A. Haury, J. Cibert, Y. Merle d'Aubigné, and A. Wasiela
Laboratoire de Spectrométrie Physique, CNRS et Université Joseph Fourier-Grenoble, Boîte Postale 87, 38402 Saint Martin d'Hères Cedex, France

J. A. Gaj
Institute of Experimental Physics, Warsaw University, 69 Hoza, 00-681 Warszawa, Poland
(Received 10 October 1995)

This paper is devoted to the description of the interface between a semimagnetic semiconductor ($Cd_{1-x}Mn_xTe$) and a nonmagnetic one (CdTe), and to the study of its magnetic and magneto-optical properties, as revealed through the enhanced Zeeman splitting of carriers confined in heterostructures. The model (proposed earlier on phenomenological bases) takes into account both the chemical profile of the imperfect interface and the enhanced magnetism due to the reduced number of magnetic neighbors at the interface. We first justify the model (for low Mn contents) by considering the statistics of Mn clusters at the interface or in a single $Cd_{1-x}Mn_xTe$ monolayer embedded in CdTe. We also show that the sensitivity of the Zeeman effect to the presence of two-dimensional islands at the interface rapidly decreases as the island width increases; i.e., the measure is sensitive to the presence of isolated magnetic ions and not (or less) to roughness, and it characterizes the interface on the scale of interatomic distance. Then we apply this tool to a wide series of samples with different nominal characteristics and different growth conditions. A unique profile (determined with a single adjustable parameter) accounts for the enhanced Zeeman splitting observed on samples grown at low temperature (250–280 °C) under excess of Cd, independently of the details of the carrier-wave function and of its penetration into the magnetic barrier: this is a further (experimental) check of the calculation. The exponential profile deduced for these samples accounts for the larger enhancement of Zeeman splitting at the inverted interface (CdTe grown on $Cd_{1-x}Mn_xTe$), compared to the normal interface ($Cd_{1-x}Mn_xTe$ on CdTe). It points to a complete exchange of Cd and Mn atoms between the two surface layers during growth (i.e., a segregation process with a segregation energy determined to be zero). We found very little influence of growth interruptions and of growing the $Cd_{1-x}Mn_xTe$ barrier under Te excess. As the growth temperature is raised above 300 °C, the interface further broadens, the additional broadening being identical for the two interfaces. Finally, we found that the Zeeman effect of carriers confined in quantum wells incorporating a magnetic inverted interface (including symmetrical quantum wells) is completely dominated by the effect of the nonabrupt profile, while a small contribution of the intrinsic effect seems to exist in a quantum well with only a normal magnetic interface or heterostructures with single $Cd_{1-x}Mn_xTe$ monolayers.

Determining and mastering the morphology of interfaces is a central problem of semiconductor heterostructures. To that purpose, a knowledge of the average profile in the *z* direction normal to the interface is not sufficient, and it is also necessary to determine a characteristic scale in the plane of the interface. A good knowledge of the morphology of an interface requires the use of several experimental tools, each of them providing a piece of information at a given scale.

For example, optical spectroscopy of quantum wells characterizes the interface morphology with the exciton coherence length (typically the Bohr radius) as a reference scale size.[1] An interface is called *smooth* if flat terraces larger than the exciton coherence length exist. Then the transition energy, which depends on the exact width of the quantum well, is well defined and the linewidth is small. If terrace widths are of the order of the exciton coherence length, strong fluctuations broaden the optical line and the interface is called *rough*. However if the lateral scale of interface fluctuations is small compared to the exciton coherence length, the energy is well averaged and the line is sharp; this is the so-called *pseudosmooth* interface. Other experimental methods have their own characteristic length. X-ray diffraction is well suited to measure smooth interface profiles of superlattices,[2] but usually gives no information on the lateral morphology except when grazing incidence is used. The same is true for Raman scattering.[3] Electron microscopy allows us to study different scales,[4] but nevertheless averages over the specimen thickness. Scanning tunneling microscopy on cleaved samples gives extremely detailed information,[5] but was not widely used until now. As already stated,[6] and justified below, magneto-optics of heterostructures incorporating semimagnetic semiconductors is very sensitive to the presence of isolated magnetic atoms: it characterizes the interface at the scale of the interatomic distance.

It has been recognized for some time that, contrary to earlier assumptions, interfaces play a key role in the magnetic properties of heterostructures with semimagnetic semiconductors as barrier material. The origin of the effect is *a priori* twofold, and the relative importance of the two contributions has been a matter of debate. First, the suppression of a fraction of the magnetic nearest neighbors at the interface is expected to enhance the magnetization[7] by reducing

the probability of forming antiferromagnetic pairs below its value in bulk material (*intrinsic effect*). Second, interfaces are not perfect, and progressive dilution across a graded interface may also be the cause of an enhanced magnetization (*extrinsic effect*). Recently we have experimentally shown the relevance of the second mechanism,[6] and proposed a scheme of calculating both the intrinsic and extrinsic contributions, starting from the experimentally known bulk magnetization and making as few assumptions as possible.[8] Results were described for several hypothetical interface profiles. In this paper we wish to (i) establish the calculation on a microscopic basis, at least for small concentrations of the magnetic atoms (<0.1, but probably also for significantly larger values), and (ii) apply the calculation to a wide series of heterostructures in order to figure out the most probable profile of as-grown interfaces. The result is that the Zeeman effect measured on all types of structures grown at low temperature (250–280 °C) agrees with a complete Cd/Mn atom exchange, during the growth of the interface, between the two surface monolayers (the one being grown and the last incorporated layer), while for samples grown at higher temperature (310–320 °C) atoms are exchanged on a larger depth.

The paper is organized as follows. First (Sec. I) we briefly recall the main experimental results which, on qualitative arguments, help in selecting the correct description of the CdTe-$Cd_{1-x}Mn_xTe$ interface grown by molecular-beam epitaxy. In Sec. II we briefly recall the method used to calculate the Zeeman splitting in a heterostructure. In Sec. III we discuss the enhanced magnetization at the interface. Then we describe and analyze the experimental results obtained on samples grown at low temperature under Cd excess (Sec. IV) and under different growth conditions (Secs. V and VI). A short discussion will be found in Sec VII.

I. QUALITATIVE EXPERIMENTAL RESULTS AND THE CHOICE OF AN INTERFACE MODEL

Several experimental results are striking enough to guide us in the choice of a correct description of interface effects.

(1) In some CdTe-$Cd_{1-x}Mn_xTe$ quantum wells (QW's) with large concentrations of Mn in the barriers ($\geqslant 0.3$) and small QW thicknesses (≈ 2 nm), the Zeeman splitting observed on excitons formed of confined carriers is larger than the splitting of the barrier exciton.[6] In an early model of such semimagnetic QW's, carriers are confined in a perfect square QW, made of pure CdTe, separated by abrupt interfaces from a $Cd_{1-x}Mn_xTe$ alloy with bulklike magnetic properties. In this description, the Zeeman effect in the barriers induces a variation of the barrier height, which itself induces a *smaller* variation of the energies of confined levels: this is measured as the Zeeman splitting in the QW, which must be smaller than in the barriers. The experimental result demonstrates without further analysis the importance of interface effects, either intrinsic or due to a smooth profile.

(2) The role of the interface profile, as opposed to an intrinsic interface effect, was stressed by several results.

(a) The larger Zeeman splitting observed on asymmetric $Cd_{1-x}Mn_xTe$-CdTe-$Cd_{1-y}Zn_yTe$ QW's with the magnetic CdTe-on-$Cd_{1-x}Mn_xTe$ interface (i.e., the so-called inverted interface being magnetic), as compared to identical $Cd_{1-y}Zn_yTe$-CdTe-$Cd_{1-x}Mn_xTe$ QWs grown in the reversed order (the so-called normal interface, $Cd_{1-x}Mn_xTe$-on-CdTe, being magnetic).[9]

(b) The increase of the Zeeman splitting for samples grown at higher temperature.[10]

(c) The increase of the Zeeman splitting upon annealing.[11]

To conclude, experimental results show, before any analysis which has to be done in the frame of a detailed model, that (i) the Zeeman effect of confined carriers is sensitive to interfaces; (ii) interfaces are not perfect, and the Zeeman effect depends on the morphology of the interface; (iii) the two interfaces of a QW, normal and inverted, are different.

II. ZEEMAN EFFECT OF CONFINED CARRIERS

A. Bulk

In this section we briefly recall the method used to calculate the Zeeman splitting of carriers in a heterostructure incorporating a semimagnetic semiconductor like $Cd_{1-x}Mn_xTe$. Further details and the discussion of the influence of material parameters are to be found in the Appendix and in Ref. 8.

In the mean-field and virtual crystal approximations, the giant Zeeman effect in bulk $Cd_{1-x}Mn_xTe$ (Ref. 12) shifts the conduction- and valence-band edges from their zero-field value by a term proportional to the average magnetization of the Mn spins in the semimagnetic semiconductor, $M_{\text{bulk}}(x,B,T)$, which depends on the Mn content x, the applied field B and the temperature T.

The magnetization (in units of $g\mu_B$) is written

$$M_{\text{bulk}}(x,B,T)=x\bar{S}(x)B_{5/2}\left[\frac{g\mu_B B}{k_B[T+T_0(x)]}\right], \qquad (1)$$

where

$$B_{5/2}(y)=\tfrac{6}{5}\coth(\tfrac{6}{5}\,y)-\tfrac{1}{5}\,\coth\left(\frac{y}{5}\right)$$

is the Brillouin function,

$$T_0(x)=\frac{35.37K}{1+2.752x}\,x,$$

$$\bar{S}(x)=S[0.265\,\exp(-43.34x)+0.735\,\exp(-6.19x)],$$

and

$$S=\tfrac{5}{2}.$$

Note that these parameters were deduced from measurements of the Zeeman splitting in bulk alloys.[8] This parametrization was checked at liquid-helium temperature, low field $B<5$ T (in particular the saturation of magnetization described by the Brillouin function is apparent and magnetization steps due to the Mn pairs are seen at higher fields), and Mn concentrations up to $x=0.67$.

The Zeeman shift of the conduction band is

$$\Delta E_{\mathrm{CB},\pm 1/2}(x,B,T) = \pm \tfrac{1}{2} N_0 \alpha M_{\mathrm{bulk}}(x,B,T)$$
$$= \pm \frac{N_0 \alpha}{2N_0(\alpha-\beta)} \Delta E(x,B,T)$$
$$= \pm 110 \text{ meV } x\bar{S}(x) B_{5/2}\left[\frac{g\mu_B B}{k_B[T+T_0(x)]}\right]. \quad (2)$$

The Zeeman shift of the heavy-hole valence band is

$$\Delta E_{\mathrm{VB},\pm 3/2}(x,B,T)$$
$$= \pm \tfrac{1}{2} N_0 \beta M_{\mathrm{bulk}}(x,B,T)$$
$$= \pm \frac{N_0 \beta}{2N_0(\alpha-\beta)} \Delta E(x,B,T)$$
$$= \mp 440 \text{ meV } x\bar{S}(x) B_{5/2}\left[\frac{g\mu_B B}{k_B[T+T_0(x)]}\right]. \quad (3)$$

In the bulk, these quantities are experimentally easy to measure, and are well known [especially the heavy-hole exciton Zeeman splitting $\Delta E(x,B,T) = N_0(\alpha - \beta) M_{\mathrm{bulk}}(x,B,T)$, leading to the commonly accepted values $N_0\alpha = 0.22$ eV and $N_0\beta = -0.88$ eV].

B. Heterostructures

The main assumption of our model[8] is to apply this *locally* at every monolayer along the growth axis of a QW in order to calculate the confining potentials in a heterostructure where the local composition varies. More precisely, at a position z along the growth axis the actual composition is $x(z)$, and this, with the conduction- and valence-band offsets, defines the potential profiles for heavy holes and electrons without applied field, $V_{\mathrm{VB},\pm 3/2}[x(z)]$ and $V_{\mathrm{CB},\pm 1/2}[x(z)]$ (see the Appendix for numerical values). These potentials include the effect of mismatch strains on the band offsets. In the presence of a magnetic field B applied along the growth axis, we add to these potentials the relevant Zeeman shifts corresponding to the *local* magnetization. Hence the potentials under applied field are

$$V_{\mathrm{CB},\pm 1/2}[x(z)] \pm \tfrac{1}{2} N_0 \alpha M_{\mathrm{local}}[x(z),z,B,T],$$
$$V_{\mathrm{VB},\pm 3/2}[x(z)] \pm \tfrac{1}{2} N_0 \beta M_{\mathrm{local}}[x(z),z,B,T], \quad (4)$$

where $M_{\mathrm{local}}[x(z),z,B,T]$ is the local magnetization at position z within the heterostructure described by its concentration profile $x(z)$.

A crucial point is to evaluate this local magnetization $M_{\mathrm{local}}[x(z),z,B,T]$ in the heterostructure. As a first approach one calculates the local magnetization in the monolayer at position z, with the concentration $x(z)$, by setting

$$M_{\mathrm{local}}[x(z),z,B,T] \approx M_{\mathrm{bulk}}[x(z),B,T], \quad (5)$$

and ignoring the difficulties arising from the concentration profile around the position z.

A better approximation, which will be justified below for small Mn contents (<0.1), is that the *magnetization per Mn spin* in the homogeneous structure depends only on the *local average probability* x_{NN} for nearest neighbor in the cation sublattice to be a Mn atom. At a (001) interface a Mn atom has four nearest neighbors in the same (001) monolayer, four in the preceding monolayer, and four in the following one. At an abrupt interface between an alloy of composition x and CdTe, one-third of the possible Mn neighbors are replaced by Cd, and $x_{\mathrm{NN}} = 2x/3$; in a $Cd_{1-x}Mn_xTe$ monolayer inserted in CdTe, $x_{\mathrm{NN}} = x/3$. If the composition changes smoothly across a broadened interface, we calculate

$$x_{\mathrm{NN}}(z) = \frac{x(z-d)+x(z)+x(z+d)}{3}, \quad (6)$$

where d is the monolayer thickness $d = 0.32$ nm. *In practice*, in a heterostructure we replace the local magnetization per spin $M_{\mathrm{local}}[x(z),z,B,T]/x(z)$ by the local magnetization per spin of the homogeneous alloy with the same number of nearest neighbors, $M_{\mathrm{bulk}}[x_{\mathrm{NN}}(z),B,T]/x_{\mathrm{NN}}$. Hence

$$M_{\mathrm{local}}[x(z),z,B,T] \approx \frac{M_{\mathrm{bulk}}[x_{\mathrm{NN}}(z),B,T]}{x_{\mathrm{NN}}(z)} x(z). \quad (7)$$

In the following we will refer to Eq. (7) as the *intrinsic model*. Equation (5) neglects this intrinsic effect and is less accurate, but remains a good approximation if the extrinsic effect (presence of broad interfaces) is dominant, i.e., $x_{\mathrm{NN}}(z) \approx x(z)$.

Thus, in the presence of the extrinsic effect only, the confining potentials with applied fields for the heavy-hole valence band and for the conduction band are written directly as

$$V_{\mathrm{VB},\pm 3/2}[x(z)] \pm 0.4 \Delta E[x(z),B,T],$$
$$V_{\mathrm{CB},\pm 1/2}[x(z)] \pm 0.1 \Delta E[x(z),B,T]. \quad (8)$$

When taking additionally the intrinsic effect into account, we use

$$V_{\mathrm{VB},\pm 3/2}[x(z)] \pm 0.4 \frac{\Delta E[x_{\mathrm{NN}}(z),B,T]}{x_{\mathrm{NN}}(z)} x(z),$$
$$V_{\mathrm{CB},\pm 1/2}[x(z)] \pm 0.1 \frac{\Delta E[x_{\mathrm{NN}}(z),B,T]}{x_{\mathrm{NN}}(z)} x(z). \quad (9)$$

Once again, the Zeeman splitting ΔE in bulk $Cd_{1-x}Mn_xTe$ is very well known experimentally. For a quantitative use of Zeeman measurements, it is essential to calculate accurately the energy of the electrons and holes confined in the potential corresponding to their spin state [Eq. (9)], and then to form the exciton: this will be done in Secs. IV and V.

When comparing the calculated exchange splitting to the observed splitting, the direct Zeeman splitting $[\sigma^- - \sigma^+ = (-0.06 \pm 0.06) \text{ meV } T^{-1} \times B]$ has to be taken into account. The values reported as experimental are obtained by substracting the direct Zeeman splitting from the observed one.

III. INTERFACE MAGNETIZATION

In this section we shall (1) use cluster statistics for low Mn contents to justify the approximation introduced above [Eq. (7)] for the estimation of the local magnetization, (2) examine the magnetization changes introduced for the three

TABLE I. Probability P_i that a Mn atom be in a cluster of i spins for atoms in a bulk alloy of composition x, for atoms at an abrupt interface between CdTe and $Cd_{1-x}Mn_xTe$, and atoms at a perfect monolayer of $Cd_{1-x}Mn_xTe$ in CdTe. $y=1-x$.

	Bulk (Ref. 13)	Interface (see also Ref. 7)	Monolayer
P_1	y^{12}	y^8	y^4
P_2	$12xy^{18}$	$4x[y^{12}+y^{14}]$	$4xy^6$
P_3^C	$24x^2y^{22}$	$4x^2[2y^{16}+y^{18}]$	0
P_3^O	$18x^2[2y^{23}+5y^{24}]$	$2x^2[6y^{15}+5y^{16}+8y^{18}+3y^{19}+10y^{20}]$	$6x^2[2y^7+y^8]$

different interfaces (monolayer, inverted interface, normal interface), and (3) consider the case of roughness with a finite lateral scale. A preliminary account was given in Ref. 13.

A. Cluster statistics

The magnetization of bulk $Cd_{1-x}Mn_xTe$, $M_{\text{bulk}}(x,B,T)$, exhibits a sublinear dependence on the Mn content x which is well known and attributed to the formation of pairs and clusters of nearest neighbors coupled by antiferromagnetic exchange. For low-Mn contents a quantitative account[14] has been given just by considering the distribution of such clusters in the homogeneous alloy of composition x. This allows us to calculate the average spin per Mn atom, at saturation, $\bar{S}(x)$. For low x it is sufficient to consider the probabilities P_i for a given spin to be in a small cluster of i spins: P_1 to be single [the 12 nearest neighbors are Cd atoms, hence $P_1=(1-x)^{12}$], P_3^O to be part of an open triplet (average spin $S_3^O=\frac{5}{6}$), and P_3^C to be part of a closed triangle (average spin $S_3^C=\frac{1}{6}$). Then the average spin is $\bar{S}=\Sigma_{i=\text{configurations}}P_iS_i=S[P_1+P_3^O/3+P_3^C/15]$ with $S=\frac{5}{2}$. Similar analytical expressions can be given for an abrupt CdTe-$Cd_{1-x}Mn_xTe$ interface and for a monolayer of $Cd_{1-x}Mn_xTe$ (Table I). For higher Mn contents a numerical computation including large clusters has been given[15] which exhibits reasonable agreement with experimental data.

We note that in this description the magnetization at saturation is proportional to $x\bar{S}$, where $\bar{S}$ is a sum over the different probabilities to find a given Mn spin embedded in a cluster. As a result, $\bar{S}$ depends on the particular geometry of the heterostructure (monolayer or single interface, orientation, interface roughness, ...) and of the successive probabilities x_{NN} of nearest neighbors, x_{NNN} of next-nearest neighbors, etc. Our approximation [leading to Eq. (7)] consists of replacing the actual $\bar{S}_{\text{local}}$, in the heterostructure, by $\bar{S}_{\text{bulk}}(x_{\text{NN}})$ in the bulk alloy of composition x_{NN}:

$$\bar{S}_{\text{local}}(x_{\text{NN}},x_{\text{NNN}},\ldots)\approx\bar{S}_{\text{bulk}}(x_{\text{NN}}); \tag{10}$$

i.e., we neglect the influence of further neighbors and of the detail of the geometry.

To check this approximation, we apply it to the cluster statistics: in Fig. 1 we plot the exact cluster probabilities $P_1(x)$, $P_2(x)$, and $P_3^C(x)+P_3^O(x)$ calculated for an atom sitting at an abrupt CdTe-$Cd_{1-x}Mn_xTe$ interface, and compare them to the $P_i(x_{\text{NN}})$ calculated for the bulk alloy of composition x_{NN}, taking $x_{\text{NN}}=2x/3$. For the case of the single $Cd_{1-x}Mn_xTe$ monolayer we have to use $x_{\text{NN}}=x/3$ and compare $P_{\text{mono}}(x)$ and $P_{\text{bulk}}(x/3)$. The very good agreement observed in Fig. 1 validates the approximation for small concentrations where cluster statistics are meaningful.

For higher x, larger and larger clusters need to be considered: above the percolation threshold x_c there is a nonvanishing probability that a given spin belongs to an infinite cluster. For bulk $Cd_{1-x}Mn_xTe$ with a three-dimensional fcc lattice, $x_c\approx0.19$, while for the $Cd_{1-x}Mn_xTe$ monolayer with a two-dimensional square lattice, $x_c=\frac{1}{2}$. However, the validity range of the approximation is probably even larger than expected from Fig. 1 for two reasons:

(i) The magnetization per spin in a large cluster decreases rapidly with the cluster size; as a result, numerical evaluations of cluster statistics quite agree with experimental magnetizations measured on bulk alloys even for high concentrations.[15] Actually, the same comparison of $\bar{S}_{\text{interface}}(x)$ calculated for the abrupt interface, and bulk $\bar{S}_{\text{bulk}}(x_{\text{NN}})$, can be done using the calculated values of Ref. 15, with a very reasonable agreement;

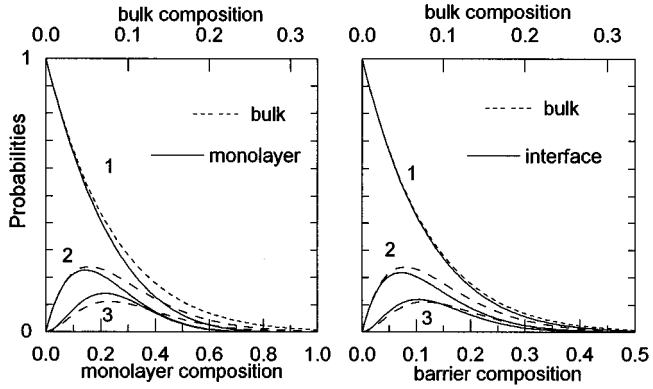

FIG. 1. Solid line: probability to be single (1), in a pair (2), or in a triangle (3) (open and closed triangles together) for a Mn atom in a monolayer (left) or at an interface (right) as function of the Mn concentration (lower axis). Dashed line: probability in the bulk alloy of uniform composition equal to the average number of nearest neighbors $x_{\text{NN}}=x/3$ (left) or $x_{\text{NN}}=2x/3$ (right) as a function of the Mn concentration (upper axis).

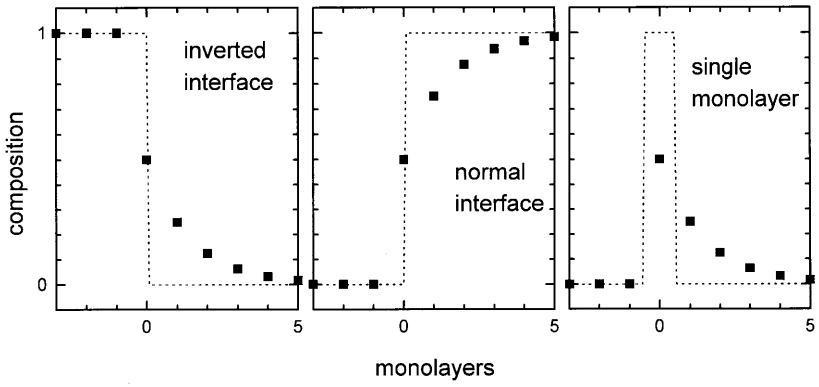

FIG. 2. Interface profile for samples grown at low temperature (closed symbols) compared to the nominal profile (dotted line). The vertical scale is in units of the nominal composition x. The zero of the horizontal axis is the last-deposited $Cd_{1-x}Mn_xTe$ layer.

(ii) The probability of presence of confined carriers rapidly decreases if the Mn content increases: hence the Zeeman splitting of confined carriers is most sensitive to the regions of the heterostructure with low-Mn contents.

B. Magnetization at the interface

We now apply the approximation [Eq. (7)], to abrupt interfaces, and to the special case of dilute interfaces where during growth a complete Cd/Mn atom exchange occurs between the monolayer being grown and the monolayer below. That means that growing one monolayer of CdTe on top of a $Cd_{1-x}Mn_xTe$ alloy results in two monolayers of alloy with the composition $x/2$, and so on. This model of interface is currently used[16] to describe segregation at the growing interface: in the general case the equilibrium between the two monolayers is given by a mass-action law. Here we take the same equilibrium composition for the two monolayers, which means that the Cd/Mn atoms *do not* segregate, but the exchange between the surface monolayer being grown and the substrate monolayer still leads to interface broadening.

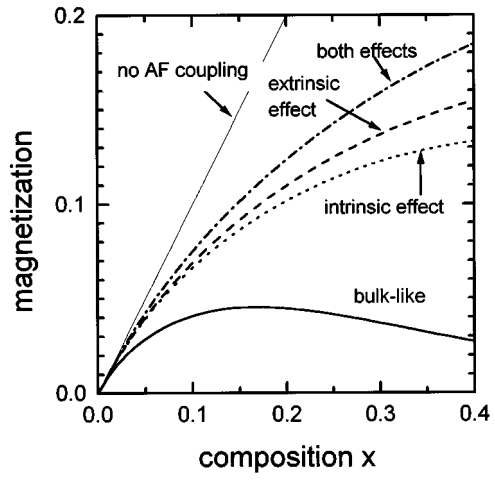

FIG. 3. Single monolayer magnetization at (apparent) saturation, calculated as a function of nominal composition. Solid line: assuming a nominal profile and neglecting the intrinsic effect. Dotted line: nominal profile taking into account the intrinsic effect. Dashed line: exponential profile, neglecting the intrinsic effect. Dot-dashed line: exponential profile, taking into account the intrinsic effect. Thin straight line: magnetization of uncoupled Mn spins. Vertical unit: 1 is one full plane of uncoupled Mn spins.

The resulting interface profile is exponential, with a tail of low-concentration alloy at the inverted interface and a steeper raise at the normal interface; in the case of a single monolayer of $Cd_{1-x}Mn_xTe$, the actual profile is a series of monolayers of decreasing concentration $x/2$, $x/4$, $x/8$,..., i.e., $x_{i+1}=x_i/2$. These profiles are shown in Fig. 2.

The following sections describe the calculated magnetization, at apparent saturation, as it could be measured in a classical magnetization measurement. For the Zeeman effect of confined carriers, described in Secs. IV–VI, ponderation by the carrier wave functions will enhance the contribution of the more diluted parts of a QW. However, in the case of superlattices with monolayers of $Cd_xMn_{1-x}Te$ inserted in CdTe (Sec. IV B), the wave function is only weakly modulated, and the Zeeman effect directly reflects the magnetization; i.e., a good estimate of the Zeeman splitting at apparent saturation is obtained by multiplying the result of Fig. 3 by $\frac{5}{2}N_0(\alpha-\beta)/p$, where p is the period of the superlattice (in ML).

1. Single monolayer

We first consider the case of a single monolayer of $Cd_{1-x}Mn_xTe$. Figure 3 shows the calculated magnetization, at apparent saturation, normalized to the magnetization of a complete monolayer of uncoupled Mn spins (i.e., $xS=1\times S=5/2$) for the following.

(i) Bulklike alloy: we use Eq. (5) with the nominal profile, and hence plot $xS(x)/S$.

(ii) Nominal profile, but taking into account the intrinsic effect: we use Eq. (7) and hence plot $xS(x_{\rm NN})/S$, with $x_{\rm NN}=x/3$.

(iii) Broadened profile: $\Sigma_i x_i \bar{S}(x_i)/S$, i.e., we use Eq. (5) and the summation runs over the successive layers with the broadened profile (Fig. 2).

(iv) Broadened profile, taking into account the intrinsic effect: $\Sigma_i x_i S[x_{\rm NN}(i)]/S$ [using Eq. (7)].

The horizontal axis is the nominal Mn concentration x.

Clearly both the existence of a broadened profile (extrinsic effect) and the intrinsic effect enhance the magnetization. However, the two effects are not additive. We conclude that, on such a structure, a large magnetization will be observed, but it would be very hazardous to attribute the observed enhancement solely to the intrinsic effect or to a smooth profile.

2. Interfaces

To discuss the case of an interface between CdTe and a thick $Cd_{1-x}Mn_xTe$ layer, we plot the difference of magneti-

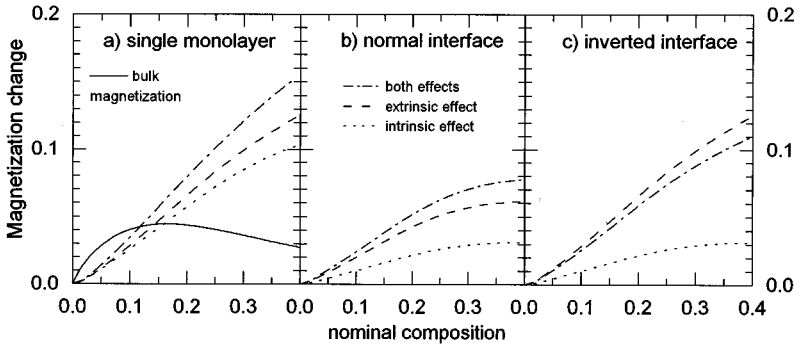

FIG. 4. Calculated magnetization change, at saturation, with respect to the nominal structure with bulk-type properties (shown as a solid line for the monolayer), at a single monolayer (a), a normal interface (b), and an inverted interface (c). Dotted lines display the intrinsic effect at an abrupt structure, dashed lines the effect of Cd/Mn atom exchange alone, and dash-dotted lines take both effects into account. (Vertical unit: 1 is one plane of uncoupled Mn spins.)

zation between the actual, broadened structure, and the abrupt interface separating pure CdTe from a $Cd_{1-x}Mn_xTe$ alloy with bulklike magnetization. This is done in Fig. 4, for both the normal and the inverted interface, and for the single monolayer to compare with. In the latter case the curves can be deduced from Fig. 3: e.g., when taking into account the intrinsic effect only the magnetization change in Fig. 4 results from the subtraction of the solid from the dotted line in Fig. 3.

As expected, all interface effects are small at low nominal concentration x. The intrinsic effect is faint indeed at an interface, and becomes significant for the single monolayer.

Note that taking into account the intrinsic effect in addition to the extrinsic one leads to a reduction of the calculated magnetization at the inverted interface, and an increase at the normal interface. This can easily be understood when we deduce from Eq. (1) an expression proportional to the curvature:

$$x_{\mathrm{NN}}(z)-x(z)=\frac{x(z+d)-2x(z)+x(z-d)}{3}\propto\frac{\partial^2}{\partial z^2}x(z). \tag{11}$$

When calculating $x(z)\bar{S}[x_{\mathrm{NN}}(z)]$ instead of $x(z)\bar{S}[x(z)]$ for a profile with a *positive* curvature, the magnetization *decreases*, since $\bar{S}(x)$ decreases monotonously with x.

C. Interface roughness

The preceding profile is typically a pseudosmooth profile: the interface is not abrupt, but the lateral scale of the fluctuations is small, and actually the model considers a succession of monolayers of laterally homogenous alloys, with a varying composition $x(z)$ which contains all the information on the interface. The influence of interface roughness—i.e., involving fluctuations of the interface at a finite scale within the interface plane—can be estimated using the same approximation.

With the growth conditions we generally use (except for a few samples grown at temperatures below 250 °C), intense oscillations of the specular reflection high-energy electron-diffraction (RHEED) spot are observed. Hence roughness with three-dimensional (3D) islands, several monolayers thick, is unlikely. We shall restrict the discussion to the case of 2D islands, one monolayer thick, with edges along 110 directions. We consider a crude model of roughness (Fig. 5): an interface between CdTe and $Cd_{1-x}Mn_xTe$, with square islands of $Cd_{1-x}Mn_xTe$ protruding into the CdTe layer, one monolayer thick, $L\times L$ in size within the plane, with a density $1/2L^2$ (i.e., there is one monolayer at the interface with an average Mn content of $x/2$, distributed in square islands of size L: the Mn composition is x within the square islands, 0 outside). We shall neglect any overlap between these islands. The interface (i.e., the part of the sample with modified properties) consists of the monolayer with the islands (which is half-filled) and the alloy monolayer immediately below: the total is $1\frac{1}{2}$ ML.

Then we can count the number of magnetic neighbors for Mn atoms within the interface monolayer ($x_{\mathrm{NN}}=8x/12$ for atoms within an island, $7x/12$ at the edge, or $6x/12$ at a corner) and for atoms in the $Cd_{1-x}Mn_xTe$ layer below the interface ($x_{\mathrm{NN}}=x$ for an atom below an island, $10x/12$ for an atom below an edge, $9x/12$ for an atom below a corner, or $8x/12$ for an atom with CdTe on top). The calculated magnetization is then

$$\frac{x}{\bar{S}}\left[\frac{(L-1)^2}{2L^2}\bar{S}(x)+\frac{4(L-1)}{2L^2}\bar{S}\left(\frac{10x}{12}\right)+\frac{4}{2L^2}\bar{S}\left(\frac{9x}{12}\right)+\frac{2L^2-6L+3}{2L^2}\bar{S}\left(\frac{8x}{12}\right)+\frac{4(L-2)}{2L^2}\bar{S}\left(\frac{7x}{12}\right)+\frac{4}{2L^2}\bar{S}\left(\frac{6x}{12}\right)\right]. \tag{12}$$

For the same quantity of Mn at a perfectly abrupt interface ($L\to\infty$: a complete monolayer below half a monolayer) we

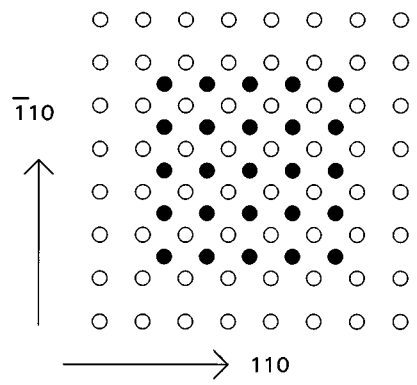

FIG. 5. Sketch of a square island of dimension 5×5 at a (001) interface. Edges are along $\langle110\rangle$ directions. Symbols represent the cations in the alloy [Cd with probability $(1-x)$ or Mn with probability x]: closed symbols are in the island, open symbols in the monolayer immediately below.

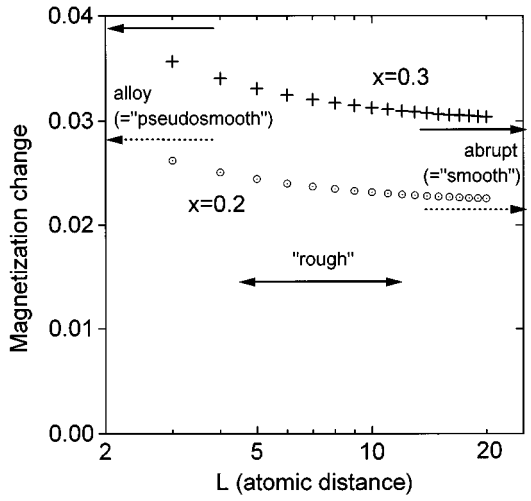

FIG. 6. Calculation of the magnetization change at saturation, with respect to the ideal interface with bulk-type properties, for a rough interface with monolayer-thick islands, as a function of the island size [Eq. (12)], for nominal compositions $x=0.2$ (circles) and $x=0.3$ (crosses). Arrows indicate the limit for an infinite-sized island [Eq. (13)], and for the alloy case [Eq. (14)]. (Vertical unit: 1 is one plane of uncoupled Mn spins.)

would have $x_{NN}=x$ for atoms under the island and $x_{NN}=8x/12$ for the other atoms in the complete $Cd_{1-x}Mn_xTe$ plane and for the island atoms; we obtain

$$\frac{x}{S}\left[\frac{1}{2}\bar{S}(x)+\bar{S}\left(\frac{8x}{12}\right)\right]. \tag{13}$$

Note that with this model we cannot modelize the transition from roughness ($L\gg 1$) down to the case of dilution (1 ML of alloy with a composition $x/2$ randomly distributed), since the alloy involves isolated atoms and a distribution of the island size should be considered. However, this crude model is enough to evaluate the effect of roughness, and the case of the alloy interface can be evaluated directly: it consists of 1 ML of composition x with $x_{NN}=10x/12$, and 1 ML of composition $x/2$ with $x_{NN}=6x/12$, hence with the reduced magnetization

$$\frac{x}{S}\left[\bar{S}\left(\frac{10x}{12}\right)+\frac{1}{2}\bar{S}\left(\frac{6x}{12}\right)\right]. \tag{14}$$

In Fig. 6 the differences between the preceding magnetizations of the rough interface [Eqs. (12)–(14)] and that of the same amount of Mn ($1+\frac{1}{2}$ML of composition x) at an interface with bulklike magnetization [i.e., $\frac{3}{2}x\bar{S}(x)/S$] are plotted as a function of the island size L. One verifies that the magnetization changes obtained for the abrupt interface are identical to those shown for the intrinsic effect in Figs. 4(b) and 4(c). Then Fig. 6 shows that the enhanced magnetization is only slightly modified, by 25%, when the interface evolves from a perfectly smooth interface to a rough interface (with one monolayer high islands of finite lateral size) and to a pseudosmooth one (with one interface monolayer having Mn concentration half the nominal concentration). In all cases the effect of roughness is negligible compared to the effect of dilution shown in Fig. 4, and it will be neglected in the following.

IV. INTERFACE AT LOW GROWTH TEMPERATURE

These samples are grown[17] by molecular-beam epitaxy at 250–280 °C, using a CdTe effusion cell which provides us with stoichiometric Cd/Te fluxes, a Mn cell, and a Cd cell to ensure an excess of metal in the beam (Cd/Te≈1.5–2).

A. Quantum wells

We have already reported[9] on the application of Zeeman studies of confined carriers to a series of asymmetric $Cd_{1-x}Mn_xTe$-CdTe-$Cd_{1-y}Zn_yTe$ quantum wells, grown in opposite order, so that for one sample the normal interface is magnetic while for the second sample it is the inverted interface which is magnetic. In addition to the structure under study, these samples include $Cd_{1-x}Mn_xTe$ and $Cd_{1-y}Zn_yTe$ layers thick enough to check the composition of the alloys by reflectance spectroscopy. The QW thicknesses are controlled by RHEED oscillations, so that all relevant parameters are accurately known in these samples.

The most striking result of the study was that the Zeeman splitting was systematically much larger for samples with an inverted magnetic interface than for samples with a normal magnetic interface (up to a factor of 3). This shows experimentally the existence of a strong effect, and that the normal magnetic interface appears much steeper than the inverted one. The interface profile could be chosen from the magnitude of the Zeeman splitting measured on samples with an inverted magnetic interface. The simplest and more probable interpretation was the model of growth generally used to describe segregation during growth by molecular-beam epitaxy. In this model the composition of the last two layers (x_i of the completed layer and x_s for the surface layer being grown) is described by a mass-action law

$$\frac{x_s(1-x_i)}{x_i(1-x_s)}=\exp\left(\frac{E_s}{k_BT}\right)=C. \tag{15}$$

In Ref. 9, the only adjustable parameter C was determined to be $C=1\pm 0.1$ (i.e., $E_s=0\pm 10$ meV at a growth temperature $T=280$ °C). This means a complete intermixing, during the growth at the interface, between the just completed monolayer and the surface monolayer being grown: the resulting monolayer concentrations decrease exponentially at an inverted interface (see Sec. III B) or increase [as $1-(1/2)^i$] toward the nominal barrier composition at a normal interface.

Henceforth we will keep $C=1$ as determined previously. We now use the same interface profile without any adjustable parameter on a wide series of asymmetric QW's with different QW widths and different compositions of the nonmagnetic barrier, and to nominally symmetric $Cd_{1-x}Mn_xTe$-CdTe-$Cd_{1-x}Mn_xTe$ quantum wells. Table II summarizes important structure parameters, and in Fig. 7 we compare the observed and calculated exchange splittings (at 1.7 K and 5 T).

To check the relevance of the interface profile we have studied quite different QW's with the inverted magnetic interface, with different QW thicknesses and different compo-

TABLE II. Parameters of the asymmetric QW's (labeled *i* for inverted magnetic interface and *n* for normal magnetic interface), symmetric QW's (labeled *S*), and superlattices (labeled SL), grown at low temperature (250–280 °C) under Cd-rich conditions. Growth interruption at the magnetic interface, if any, is performed in the vacuum. The concentrations x_{Zn} of the nonmagnetic barrier is given for the asymmetric QW's. Unless specified, exchange splittings are measured at 1.7 K and 5 T.

Sample	Growth temperature (°C)	Magnetic barrier thickness (nm)	QW thickness (nm)	Barrier composition Zn	Barrier composition Mn	Exchange splitting (meV) measured	Exchange splitting (meV) calculated
322*i*	280	2.56	6.78	0.140	0.38	2.8 (at 4 T)	2.6 (at 4 T)
323*n*	280	2.56	6.98	0.141	0.38	0.8 (at 4 T)	0.5 (at 4 T)
336*i*	280	1.92	4.67	0.112	0.35	4.3	4.3
340*n*	280	1.92	4.32	0.117	0.32	1.7	1.7
496*i*	280	1.95	4.74	1	0.37	10.8±0.15	11.4
420*i*	250	1.92	4.7	0.121	0.28	4.3	4.7
163*S*	280	>20	6.5	none	0.23	7.3	7.5
177*S*	280	>20	6.5	none	0.24	7.6	7.4
178*S*	250	>20	6.5	none	0.21	6.5	7.7
207*S*	250	>20	6.5	none	0.20	8.0	7.8
337*i*	280	0.32 (1 ML)	4.77	0.109	0.34	7.0	6.6
341*n*	280	0.32 (1 ML)	4.35	0.119	0.33	6.4	5.8
422 SL	280	0.32 (1 ML)	1.3	none	0.28	75.3	74.8
497 SL	280	0.35	1.79	none	0.34	66.5	63.4

sitions of the nonmagnetic barrier. The first four samples in Table II are representatives of the former series[9] which was grown at 280 °C, under excess Cd flux (the typical metal/Te flux ratio was from 1.5 to 2). In the valence band the confining potential of the nonmagnetic barrier is much lower than for the magnetic barrier: this results in a significant penetration of the confined heavy holes into the nonmagnetic

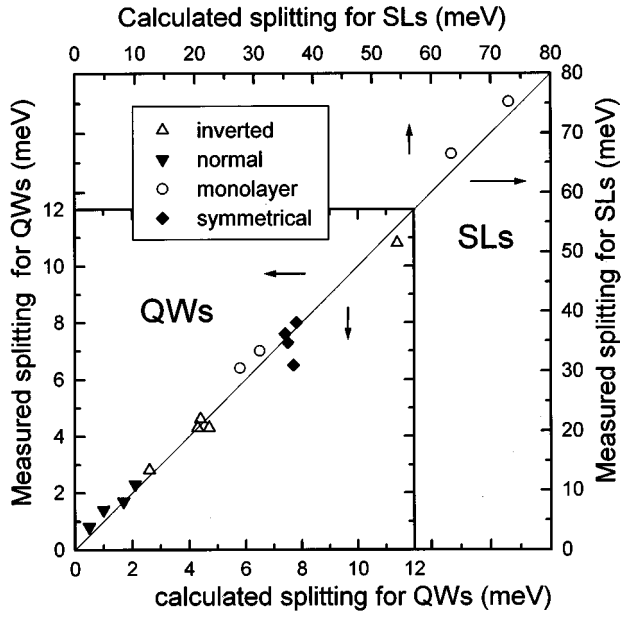

FIG. 7. Comparison between the calculated and measured exchange splittings. Samples: asymmetric QW's with inverted (up triangles) or normal (down triangles) magnetic interfaces; symmetrical QW's (diamonds); quantum wells with a single magnetic monolayer (circles); and superlattices (circles). The solid line is the exact agreement. Note the different scales for the QW's (lower and left scales) and SL's (top and right scales).

$Cd_{1-y}Zn_yTe$ barrier. In order to probe the profile deeper into the magnetic barriers, higher zinc concentrations are needed. This had been done in sample 496*i* where a 4-ml thick ZnTe barrier was deposited after the QW. As a result, the observed splitting rises to 10.8 meV still in good agreement with the calculated value of 11.4 meV.

When reducing the temperature from 280 to 250 °C the profile is not expected to change since, in Eq. (6), E_s has been determined close to 0. This is confirmed by the observation on sample 420*i*, where the splitting is still in agreement with the calculations assuming the interface profile of samples grown at 280 °C.

In these inverted QW's the Zeeman effect of confined carriers is dominated by the effect of dilution of Mn into the QW (effect of profile), as already suggested by Fig. 4. On QW's with a normal interface, on the contrary, the extrinsic effect becomes very small; as the intrinsic effect at a single interface is small, the total Zeeman splitting is small and probably more affected by uncertainties. However, the agreement between calculated and measured splittings is good.

The following four samples in Table II and Fig. 7 are symmetrical QW's where the inverted and normal interfaces simultaneously contribute to the observed splitting. When comparing with a pair of symmetric QW's, it is obvious that the dominant part of the splitting in a symmetrical QW is provided by the extrinsic effect at the inverted interface. Thus symmetrical QW's are a good test of the interface profiles—even if less selective than asymmetric QW's—and validate the interface profile for lower Mn concentrations around 0.20–0.24. The symmetrical QW's all have a 20 ML CdTe QW, but were not grown during successive runs and not always controlled by RHEED oscillations, which probably explains the dispersion of the observed splittings.

B. Structures with single monolayers of $Cd_{1-x}Mn_xTe$

If only one monolayer of the magnetic alloy is grown, the distinction between the normal and inverted interfaces may

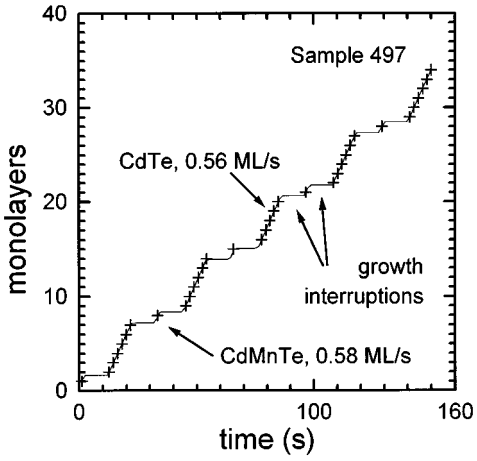

FIG. 8. Intensity minima of the RHEED oscillations during the growth of superlattice sample 497 (crosses) as a function of processing time. The horizontal steps are due to the growth interruptions. From the fit we deduce the growth rates of the two materials and the superlattice period $p = 6.74$ nm.

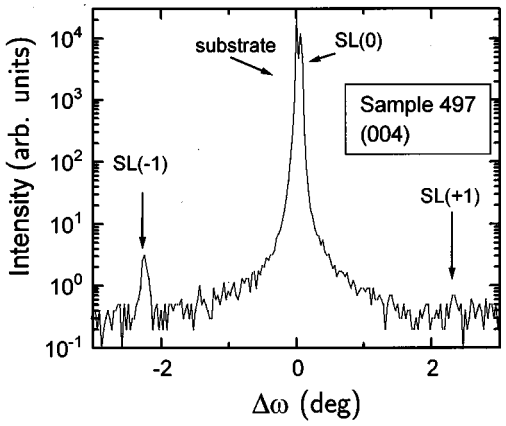

FIG. 9. (004) x-ray-diffraction profile for the same superlattice as in Fig. 8. The position of the satellite peaks gives the superlattice period $p = 6.76$ nm.

appear as academic. However, for the actual profile the amount of Mn diluted into the QW is larger if the $Cd_{1-x}Mn_xTe$ monolayer is inserted at the inverted interface of a $Cd_{1-x}Zn_xTe$-CdTe-$Cd_{1-x}Zn_xTe$ QW, than if it is located at the normal interface. This effect is observed on samples 337*i* and 341*n* (Table II). The difference is quite weak, since in this case the influence of the intrinsic effect becomes significant.

The exact amount of Mn inserted in a single $Cd_{1-x}Mn_xTe$ monolayer is easier to control if a whole CdTe-$Cd_{1-x}Mn_xTe$ superlattice is grown.[18] The whole superlattices were grown under Cd excess at 280 °C; $Cd_{1-x}Mn_xTe$ was obtained by simply adding a Mn flux. Growth was interrupted for 10 s in the vacuum at each interface. Before the growth of the superlattice, the buffer layer was annealed at 340 °C under Cd flux for several minutes: this results in intense RHEED oscillations which can be followed throughout the growth of the first few periods of the superlattice (Fig. 8), and fitted with two *a priori* different growth rates for CdTe and $Cd_{1-x}Mn_xTe$ (which, as expected for these growth conditions, are found to be nearly identical). This gives a first value of the superlattice period, obtained *in situ*. Note that at the end of the growth of the 300-period-thick superlattice, RHEED oscillations are still observed, but they are weaker and due to the small perturbation induced by the growth interruption and/or change of flux stoichiometry. As a result the oscillations lose their phase across the interfaces, and appear identical from one period to another. Hence the only information from the RHEED oscillations recorded at the end of the superlattice is that the CdTe growth rate did not vary during the growth; there is no information about the barrier thickness and the period. The layer thicknesses reported in Table II are those deduced from the RHEED recorded at the beginning of the superlattice growth.

The fact that at the beginning of the superlattice growth the period could be measured (i.e., the phase of the RHEED oscillation was conserved through the interface) was checked by x-ray diffraction (Fig. 9). The position of the satellite peak corroborated the period measured by RHEED.

Finally the alloy composition was determined from the zero-field position of the reflectance peak. Calculation showed that the very short period of the superlattice induces only very small modulations of the envelope wave function. The optically determined composition well agrees with the preliminary calibration through the relative growth rates of CdTe and MnTe on a test sample. Hence, on such a sample, the two relevant growth parameters (superlattice period and Mn content) are consistently determined using independent methods.

A very pronounced structure of the heavy-hole exciton was observed in reflectance measurements.[18] Under magnetic field the light-hole transition separated for the heavy-hole transition, as expected from the spin ratio. Here again, the calculated splittings are in very good agreement with the measured ones (Fig. 7 and Table II).

To conclude this section, the results obtained on samples grown at low temperature under Cd excess are summarized in Fig. 7. The assumed profile of the magnetic interface has been probed by carriers with different wave functions. They range from steep and weakly penetrating (samples with $Cd_{1-x}Zn_xTe$ as the nonmagnetic barrier) over deeply penetrating (samples with ZnTe as the nonmagnetic barrier) to equally averaging (superlattices). The observed Zeeman splittings cover more than two orders of magnitude, and are in agreement with calculations using a *single* interface profile.

V. GROWTH AT HIGHER TEMPERATURE

We have already shown[10] that samples grown at higher temperature exhibit a larger Zeeman splitting. In this first analysis, however, very little was known on the interface profile, and in particular the strong difference between the normal and inverted interfaces was not taken into account.

To elucidate this point we have studied asymmetric $Cd_{1-x}Mn_xTe$-CdTe-$Cd_{1-y}Zn_yTe$ QW's, grown in opposite order at 320 °C, under excess Cd (Table III). The measured Zeeman splitting, when compared to the splitting calculated in the preceding model, is slightly larger for the sample with

TABLE III. Parameters of structures grown at high temperature (310–320 °C). Calculated splittings (at 5 T and 1.7 K) are obtained in the model valid for low-temperature growth.

Sample	Growth temperature (°C)	Magnetic barrier thickness (nm)	QW thickness (nm)	Barrier composition Zn	Barrier composition Mn	Exchange splitting (meV) measured	Exchange splitting (meV) calculated (low T)
463*i*	320	1.66	4.96	0.13	0.39	5.4	4.5
462*n*	320	1.76	5.44	0.12	0.33	2.6	1.2
514 SL	320	0.32 (1 ML)	4.8	none	0.5	32 (Ref. 19)	22.5
162*S*	310	>20	6.5	none	0.24	9.3	7.4
97*S*	310	>20	6.5	none	0.32	9.9	6.9

the inverted interface, and definitely larger for the sample with the normal interface.

A first attempt would be to use the segregation model again, with a segregation coefficient C different from unity: to fit the experimental result we must increase C up to 1.2 for the inverted interface, and up to 4 for the normal interface; such a difference between the two interfaces is hard to imagine in a simple segregation model (and actually at low temperature we found $C=1$, i.e., a vanishing activation energy, so that one expects no temperature dependence in the narrow range considered here).

Instead of changing C we may notice that in the pair of samples grown at higher temperature the ratio in Zeeman splittings (463*i* over 462*n*) tends to unity, which means that the interfaces become more similar. This suggests trying a profile obtained by convoluting the preceding one (exponential) by an additional profile (Lorentzian, Gaussian, binomial, etc.). Because it is particularly easy to introduce the numerical calculation, we chose a binomial profile $f_n(i)$, which may describe interdiffusion that takes place either after the growth of the interface, or even during the growth of the interface over more than two monolayers:

$$f_n(i)=\frac{n!}{i!(n-i)!}\,2^{-n}, \tag{16}$$

where i labels the successive monolayers, and $n+1$ is the total number of monolayers affected by this additional broadening.

Figure 10 shows the Zeeman splitting calculated for four samples, after convolution of the exponential profile by binomial profiles of increasing width $\Delta=\sqrt{n}/2$ (square root of the second central moment). The series comprises two symmetrical QW's (grown at 310 °C), a pair of asymmetric QW's, and a superlattice.[19] One observes that a good fit is observed with the common value $\Delta=1.3$ ML for the two asymmetric QW's, with normal and inverted interfaces, and for the CdTe-$Cd_{0.5}Mn_{0.5}$Te superlattice, which were all grown at 320 °C; a slightly smaller value $\Delta=1.1$ ML is needed, as expected, for symmetrical CdTe-$Cd_{0.2}Mn_{0.2}$Te samples grown at 310 °C.

Figure 11 shows the resulting profile for samples grown at 320 °C, i.e., the convolution of the low-temperature profile by a symmetrical broadening (binomial distribution). At the inverted interface, the hole wave function tests the right-hand tail of the distribution; it is easily shown that there the tail of the profile is merely shifted, and this has only a small effect on the Zeeman splitting. At the normal interface, conversely, the hole wave function tests the part which was quite steep at low temperature, but is now significantly softened, resulting in an increase of the Zeeman splitting.

VI. INTERFACES GROWN UNDER Te

One possible way to reduce the cation exchange during growth could be to change the excess flux from Cd to Te.[20] However, samples grown with the Te-rich surface [i.e., the (2×1) reconstruction] usually have a rough surface and feature less intense and broader reflectance spectra. In order to inhibit the development of excessive roughness, we have grown only the $Cd_{1-x}Mn_x$Te alloy and the interfaces under excess Te flux, the Cd excess being restored during the growth of the CdTe QW's.

Then good RHEED oscillations are observed during the whole growth of a 300-period CdTe-$Cd_{1-x}Mn_x$Te superlattice. Once again, during the first few periods of the superlattice, the phase of the RHEED oscillation seems to be preserved across the interface, and here again we can follow the oscillations over several periods and try to obtain an *in situ* measure of the superlattice period. However, the period measured by x-ray diffraction is now 0.6±0.2 ML larger than the period deduced from RHEED oscillations. This has to be

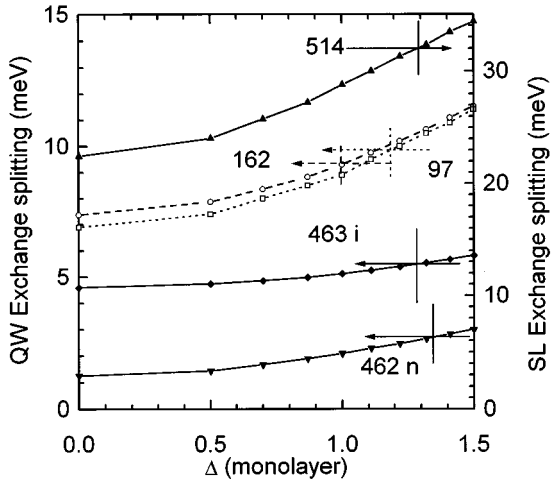

FIG. 10. Calculated exchange splittings of the QW's (left axis) and superlattice (right axis) grown at 320 °C (closed symbols) and 310 °C (open symbols): asymmetric QW's 463*i* (diamonds), 462*n* (down triangles), symmetrical QW 162 (circles) and 97 (squares), and SL 514 (up triangles), as a function of the binomial distribution width Δ (square root of variance). Experimental values are indicated by arrows.

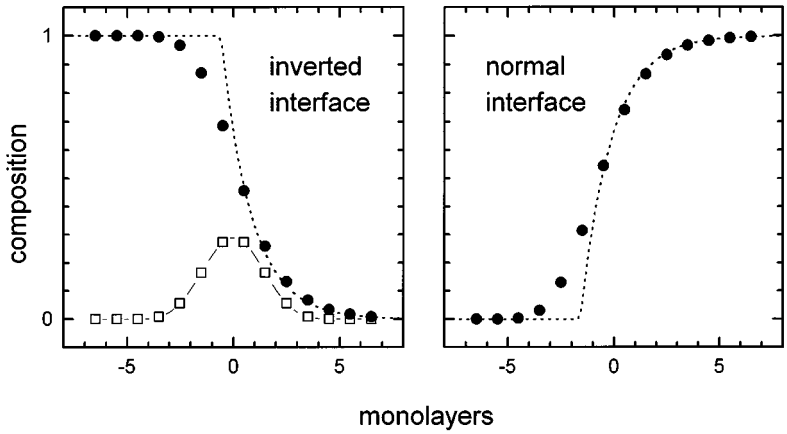

FIG. 11. Interface profile for samples grown at low temperature (dotted line) and at 320 °C (closed symbols). The high-temperature profile is obtained by convoluting the low-temperature profile (exponential function) by the binomial distribution of width $\Delta = 1.3$ ML [i.e., $n = 7$ in Eq. (16)] shown by open squares. Origins of horizontal axes have been shifted to show the identity of the low-composition tails at the inverted interface.

related to the periodic change of surface stoichiometry: at each period, we shift from a Cd-rich $c(2\times2)$ surface, with $\frac{1}{2}$ ML of Cd at the surface, to a Te-rich (2×1) surface, with 1 ML of Te at the surface,[21] and back. That means that we add $\frac{1}{2}$ ML of Cd when we shift from the (2×1) $Cd_{1-x}Mn_xTe$ surface to the $c(2\times2)$ CdTe surface, and $\frac{1}{2}$ ML of Te when we shift back from the $c(2\times2)$ CdTe surface to the (2×1) surface: the total is $\frac{1}{2}$ ML of CdTe added per period. The same amount ($\frac{1}{2}$ ML of CdTe per period) is observed in atomic layer epitaxy of CdTe,[22] and even during the sublimation of CdTe under thermal cycling between the same reconstructions.[21] However, the main point here is not this half-monolayer added per cycle, which is well explained by the stoichiometry of the two surfaces, but the fact that is not observed in the RHEED oscillation: hence the surface structure (step distribution) appears to be unchanged by a single change from the (2×1) to the $c(2\times2)$ surface, or a single change from the $c(2\times2)$ to the (2×1) surface.

As can be seen on the samples in Table IV, the Te excess flux and the growth interruptions under Te flux do not significantly inhibit the cation exchange during growth. In addition to this, the structures exhibit broader lines in reflectance measurements than the structures entirely grown under excess Cd flux.

VII. DISCUSSION AND CONCLUSIONS

The study of the enhanced Zeeman effect of excitons in CdTe-$Cd_{1-x}Mn_xTe$ heterostructures bears much information on the nature and the magnetic properties of the interface. A quantitative study was allowed by using a simplified model with two main assumptions.

(i) The interface can be described by successive layers of a $Cd_{1-x}Mn_xTe$ alloy with a varying composition $x(z)$ (pseudosmooth interface).

(ii) The local magnetization in the inhomogeneous material is mainly determined by the probability x to find a spin and the average probability x_{NN} than a nearest neighbor be magnetic.

These two assumptions allow us to describe the effect of an interface using well documented expressions [Eq. (1)] for the magnetization of bulk $Cd_{1-x}Mn_xTe$. Within the frame of this model, we have shown that the Zeeman effect of confined excitons is only weakly enhanced by roughness (in the form of the two-dimensional islands): roughness only cannot explain the enhanced Zeeman effect observed on our samples and on the samples from other groups. On the other hand, transmission electron microscope studies of MnTe layers[23] have revealed that some roughness develops as the thickness of the MnTe layer increases. These layers were grown under a Te excess (under growth conditions where RHEED intensity oscillations were not observed). Such a roughness is highly unlikely in the samples of the present study where strong RHEED oscillations were usually observed. The pseudosmooth nature of the interface is also supported by the shape and sharpness of the optical transitions. However, some broadening of the optical lines[10] (and the fact that RHEED oscillations are less easily observed) suggests that a more developed roughness exists in the samples grown at low temperature (<280 °C). From the present study, such a

TABLE IV. Parameters of structures partially grown under Te-rich conditions. Splittings are measured at and calculated for 5 T and 1.7 K.

Sample	Growth temperature (°C)	Magnetic barrier thickness (nm)	QW thickness (nm)	Barrier composition Zn	Barrier composition Mn	Exchange splitting (meV) measured	Exchange splitting (meV) calculated
459*i*	280	2.08	5.76	0.12	0.35	3.3	3.5
460*n*	280	0.32 (1 ML)	5.44	0.12	0.34	5.9	5.6
493*i*	280	1.76	6.40	1	0.33	5.2	6.1
494*i*	280	1.73	4.80	1	0.34	11.1	11.4
469 SL	280	0.32	1.52	none	0.35	67	70.9
495 SL	280	0.48	1.85	none	0.27	65.7	60.2

roughness would not alter the value of the Zeeman splitting. Roughness also is quite probable in samples entirely grown under a Te excess, which may exhibit very small values of Zeeman splitting,[20] but also exhibit broader optical transitions and no RHEED oscillations during the growth. In those samples ($Cd_{1-x}Mn_xTe$ grown at low temperature, MnTe, heterostrutures entirely grown under Te excess) the total width of the interface would include a contribution from roughness in addition to the profile deduced from the Zeeman splitting.

The scheme proposed for the calculation of the enhanced Zeeman effect, and the assumptions which permit the calculation, are validated both theoretically (statistics of Mn clusters in the heterostructure) and experimentally (study of a large series of samples with very different penetrations of the wave functions into the $Cd_{1-x}Mn_xTe$ barriers). Of course the pertinence of cluster statistics is questionable for alloys with a large Mn content; however, the probability of presence of the confined carriers is larger where the Mn content is smaller, and this may extend the usefulness of the present calculation to heterostructures including alloys with high Mn content together with CdTe. In this case one should keep in mind that the value of the Zeeman splitting carries no or little information on the Mn-rich parts of the sample: it is mostly sensitive to the tail of Mn concentration extending into the CdTe. Other methods or other types of heterostructures must be considered (with great care to the possible contribution of the interface) if the low-dimensional magnetic properties of the alloy itself are to be studied.[24,25]

An exponential $x(z)$ function is the most likely profile for samples grown at low temperature: this single profile accounts for the Zeeman splittings measured on samples with only the inverted (CdTe-on-$Cd_{1-x}Mn_xTe$) interface, the normal ($Cd_{1-x}Mn_xTe$-on-CdTe) one, both normal and inverted interfaces, or single $Cd_{1-x}Mn_xTe$ monolayer embedded in CdTe, grown at 250–280 °C. This exponential profile induces a larger enhancement of the Zeeman effect of confined excitons at the inverted interface (with a long tail of highly diluted Mn) than at the normal interface (with a steeper rise of the Mn concentration). Note, however, that other methods where Cd and Mn would be treated on the same footing (e.g., measurement of the chemical contrast in transmission electron microscopy) would not conclude for such a profile that the normal interface is more abrupt than the inverted one.

This profile naturally arises if during the growth a complete equilibrium takes place, with the same composition, between the last two surface monolayers (the surface being grown and the last incorporated monolayer). This model is currently used to describe segregation during growth by molecular-beam epitaxy,[16] but in the case of CdTe/MnTe we determine the segregation energy to be zero, i.e., there is no segregation. It has been noted elsewhere[9] that no segregation takes place also in the Bridgman growth (at higher temperatures) of bulk $Cd_{1-x}Mn_xTe$.[26] Hence the CdTe/$Cd_{1-x}Mn_xTe$ interface appears steeper than the GaAs-$Ga_{1-x}In_xAs$ interface, where segregation of In out of the growing $Ga_{1-x}In_xAs$ alloy broadens the interface, and slightly broader than the GaAs-$Ga_{1-x}Al_xAs$ interface,[3] where either segregation or incomplete equilibrium between the two surface layers[27] allows steeper interfaces.

Interfaces grown at 320 °C exhibit an additional broadening. This broadening is detected mostly at the normal interface, which strongly suggests that it is symmetrical across the interface (and hidden at the inverted interface by the preceding mechanism). We have used a binomial distribution, but the exact shape of course is not known. One possible mechanism is that at high temperature the exchange of Cd/Mn atoms, which already exists at 250 °C, takes place over more than two monolayers when the growth temperature is raised. As expected, this additional broadening is smaller in samples grown at 310 °C; it is probably already present, even if too weak to be measured, in samples grown at 280 °C.[10] Bulklike interdiffusion occurring during the whole growth of the top barrier seems to be ruled out by the low interdiffusion coefficient measured in annealing experiments.[11,28] Also a symmetrical further broadening is supported here by the study of the pair of asymmetric wells, while in Ref. 29 it was concluded that a simple exponential profile seemed to work better than a convolution with a Gaussian one in the analysis of samples annealed at 450 °C. In the case of growth at high temperature, interdiffusion may be faster within the first few monolayers below the surface, and hence stronger during growth immediately after the growth of the interface, than during the post-growth annealing of a deeply buried interface.

The intrinsic effect (due to the lack of magnetic neighbors even at an abrupt interface) is introduced in our calculation by the fact that the local magnetization is taken to be proportional to $x\bar{S}(x_{NN})$, where x_{NN} is the average probability to have a magnetic neighbor. Two conclusions follow from the present study.

(i) At the inverted interface, the extrinsic effect (smooth profile) severely masks the intrinsic contribution. Actually, due to the positive curvature of $x(z)$ at the inverted interface, the average probability that a nearest neighbor is magnetic, x_{NN}, is larger than $x(z)$, so that the intrinsic effect *reduces* the magnetization. The profile effect at the inverted interface also dominates if both interfaces are present, such as in a symmetrical QW (Ref. 7) from which very little can be learned about the intrinsic effect.

(ii) At the normal interface, and on single monolayers, a sizable contribution of the intrinsic effect appears, and its order of magnitude agrees with the result of our calculation; however, improved interfaces are still needed for a truly quantitative study.

Atomic layer epitaxy, or migration enhanced epitaxy, where metal (Cd, Mn) and Te are sent separately and allowed to diffuse on the surface,[22] could be a good way both to understand the role of the different surface reconstructions in determining the step distribution at the growing surface and the interface profile,[30] and to achieve more abrupt interfaces by limiting the exchange of Cd and Mn atoms.

ACKNOWLEDGMENTS

We are greatly indebted to G. Feuillet, H. Ulmer, and F. Kany, who made their spectroscopic measurements available to use prior to publication, and for extensive discussions and collaboration. X-ray measurements performed by A. Shen are gratefully acknowledged.

APPENDIX

Calculations were made using the following values of the effective masses along the (001) growth direction: $m_e^* = 0.096$ for electrons and $m_h^* = 0.51$ for heavy holes; the valence-band offset ratios for $Cd_{1-x}Mn_xTe$ and $Cd_{1-y}Zn_yTe$ were $\alpha_{Mn} = 0.3$ and $\alpha_{Zn} = 0.06$, respectively.

The values of the band gap E_g of $Cd_{1-x}Mn_xTe$ and $Cd_{1-y}Zn_yTe$ were

$$E_g^{Cd_{1-x}Mn_xTe}(x) = 1.606\ \text{eV} + 1.592\ \text{eV} \times x,$$

and

$$E_g^{Cd_{1-y}Zn_yTe}(y) = 1.606\ \text{eV} + 0.525 \times y + 0.26\ \text{eV} \times y^2.$$

Lattice parameters were taken from Ref. 31. We assumed (after calculations of Ref. 32) a ratio of hydrostatic deformation potentials of conduction and valence band $a_c/a_v = -2$ and, since we are concerned with relatively low mole fractions, we take the deformation potentials of CdTe:[33,34]

$$a = -3.85\ \text{eV} \quad \text{and} \quad b = -1.15\ \text{eV} \quad \text{for CdTe},$$

$$a = -5.48\ \text{eV} \quad \text{and} \quad b = -1.3\ \text{eV} \quad \text{for ZnTe}.$$

For MnTe we take the same values as for CdTe. The elastic constants are those of Ref. 35.

Our structures were grown either on thick buffer layers of the $Cd_{1-x}Mn_xTe$ barrier material (in the case of nominally symmetric QW's) or on $Cd_{1-y}Zn_yTe$ buffers with concentrations y_{nom} lattice matched to the nominal $Cd_{1-x}Mn_xTe$ barrier concentration x_{nom} (for asymmetric QW's) ($x_{nom}/y_{nom} = 2.7$). In the presence of a given Mn concentration x and Zn concentration y at a given point z along the growth axis, the conduction and valence-band potential profiles can be written as

$$V_{CB,\pm 1/2} = 1.606\ \text{eV} + 1.1144\ \text{eV} \times x + 0.0336\ \text{eV} \times (x_{nom} - x) + 0.4935\ \text{eV} \times y + 0.2444\ \text{eV} \times y^2 + 0.0903\ \text{eV} \times (y_{nom} - y),$$

$$V_{VB,\pm 3/2} = 0.4776\ \text{eV} \times x + 0.0433\ \text{eV} \times (x_{nom} - x) + 0.0315\ \text{eV} \times y + 0.0156\ \text{eV} \times y^2 + 0.1152\ \text{eV} \times (y_{nom} - y).$$

The exciton binding energy was calculated using the model of Ref. 36. When comparing the calculated exchange splitting to the observed splitting, the direct Zeeman splitting $[\sigma^- - \sigma^+ = (-0.06 \pm 0.06)\ \text{meV}\ T^{-1} \times B]$ has to be taken into account. The values reported as experimental are also obtained by subtracting the direct Zeeman splitting from the observed one.

Calculations[37] using other Luttinger parameters [leading to $m_h^* = 0.72$ along (001)] and including the effect of strain on the QW width, lead to slightly higher (+0.08) values of C, and confirm the weak dependence of our conclusions on calculation parameters demonstrated in Ref. 8.

[1] R. K. Kopf, E. F. Schubert, T. D. Harris, and R. S. Becker, Appl. Phys. Lett. **58**, 631 (1991); D. Gammon, B. V. Shanabrook, and D. S. Katzer, Phys. Rev. Lett. **67**, 1547 (1991).

[2] R. M. Fleming, D. B. McWhan, A. C. Gossard, W. Wiegman, and R. A. Logan, J. Appl. Phys. **51**, 357 (1980).

[3] B. Jusserand and F. Mollot, Appl. Phys. Lett. **61**, 423 (1992).

[4] A. Ourmazd, D. W. Taylor, J. Cunningham, and C. W. Tu, Phys. Rev. Lett. **62**, 933 (1989).

[5] M. B. Johnson, U. Maier, H. P. Meier, and H. W. M. Salemink, Appl. Phys. Lett. **63**, 1273 (1993).

[6] J. A. Gaj, C. Bodin, P. Peyla, J. Cibert, G. Feuillet, Y. Merle d'Aubigné, R. Romestain, and A. Wasiela, in *Proceedings XXI ICPS, Beijing, 1992*, edited by Ping Jiang and Hou-Zhi Zheng (World Scientific, Singapore, 1992), p. 1936.

[7] W. J. Ossau and B. Kuhn-Heinrich, Physica B **184**, 422 (1993).

[8] J. A. Gaj, W. Grieshaber, C. Bodin, J. Cibert, G. Feuillet, Y. Merle d'Aubigné, and A. Wasiela, Phys. Rev. B **50**, 5512 (1994).

[9] W. Grieshaber, J. Cibert, J. A. Gaj, Y. Merle d'Aubigné, and A. Wasiela, Phys. Rev. B **50**, 2011 (1994).

[10] W. Grieshaber, C. Bodin, J. Cibert, J. Gaj, Y. Merle d'Aubigné, A. Wasiela, and G. Feuillet, Appl. Phys. Lett. **65**, 1287 (1994).

[11] J. Gaj, J. Cibert, G. Feuillet, W. Grieshaber, G. Karczewski, P. Kossacki, Y. Merle d'Aubigné, Nguyen The Koi, A. Wasiela, and T. Wojtowicz, in *Proceedings of the 11th International Conference on High Magnetic Fields in the Physics of Semiconductors, "SEMIMAG-94," Cambridge, 1994*, edited by Don Heiman (World Scientific, Singapore, 1995), p. 638.

[12] J. A. Gaj, R. Planel, and G. Fishman, Solid State Commun. **29**, 435 (1979); J. K. Furdyna, J. Appl. Phys. **64**, R29 (1988), and references therein.

[13] J. Cibert, W. Grieshaber, J. A. Gaj, Y. Merle d'Aubigné, and A. Wasiela, Mater. Sci. Forum **18**, 567 (1995).

[14] Y. Shapira, S. Foner, D. H. Ridgley, K. Dwight, and A. Wold, Phys. Rev. B **30**, 4021 (1984).

[15] J. M. Fatah, T. Piorek, P. Harrison, T. Stirner, and W. E. Hagston, Phys. Rev. B **49**, 10 341 (1994).

[16] J. M. Moison, C. Guille, F. Houzay, F. Barthe, and M. Van Rompay, Phys. Rev. B **40**, 6149 (1989).

[17] C. Bodin, J. Cibert, W. Grieshaber, Le Si Dang, F. Marcenat, A. Wasiela, P. H. Jouneau, G. Feuillet, D. Hervé, and E. Molva, J. Appl. Phys. **77**, 1069 (1995).

[18] Y. Merle d'Aubigné, W. Grieshaber, J. Cibert, A. Wasiela, and J. A. Gaj, in *Proceedings of the XXII International Conference on the Physics of Semiconductors—Vancouver*, edited by D. J. Lockwood (World Scientific, Singapore, 1994), p. 2601.

[19] F. Kany, H. Ulmer, and G. Feuillet, *Proceedings of the International Conference on Semiconductor Heteroepitaxy—Montpellier* (World Scientific, Singapore, 1996).

[20] S. Kuroda, K. Kojima, K. Kobayashi, A. Saito, K. Takita, K. Uchida, and N. Miura, Mater. Sci. Forum **18**, 615 (1995).

[21] S. Tatarenko, F. Bassani, J. C. Klein, K. Saminadayar, J. Cibert, and V. H. Etgems, J. Vac. Sci. Technol. A **12**, 140 (1994).

[22] W. Faschinger and H. Sitter, J. Cryst. Growth **99**, 566 (1990).

[23] P. H. Jouneau, A. Tardot, G. Feuillet, H. Mariette, and J. Cibert, J. Appl. Phys. **75**, 7310 (1994).
[24] D. D. Awshalom, J. Warnock, and S. von Molnar, Phys. Rev. Lett. **58**, 812 (1987).
[25] M. Sawicki, T. Dietl, G. Karczewski, T. Wojtowicz, and J. Kossut, Mater. Sci. Forum **18**, 685 (1995).
[26] R. Triboulet and G. Didier, J. Cryst. Growth **52**, 614 (1981).
[27] O. Dehaese, X. Wallart, and F. Mollot, Appl. Phys. Lett. **66**, 52 (1995).
[28] D. Tönnies, G. Bacher, A. Forchel, A. Waag, and G. Landwehr, Appl. Phys. Lett. **64**, 766 (1994).
[29] P. Kossacki, Nguyen The Koi, J. A. Gaj, G. Karczewski, T. Wojtowicz, E. Janik, A. Zakrewski, M. Kutrowski, and J. Kossut, Superlatt. Microstruct. **16**, 63 (1994).
[30] J. M. Hartmann, G. Feuillet, H. Mariette, J. M. Vaca, and M. Charleux, *Proceedings of the International Conference on Semiconductor Heteroepitaxy—Montpellier* (Ref. 19).
[31] J. K. Furdyna, J. Appl. Phys. **64**, R29 (1988).
[32] D. L. Camphausen, G. A. N. Connel, and W. Paul, Phys. Rev. Lett. **26**, 184 (1971).
[33] D. G. Thomas, J. Appl. Phys. **32**, 2298 (1961).
[34] Y. Merle d'Aubigné *et al.*, J. Cryst. Growth **101**, 650 (1990).
[35] R. D. Greenough and S. B. Palmer, J. Appl. Phys. D **6**, 587 (1973).
[36] P. Peyla, Y. Merle d'Aubigné, A. Wasiela, R. Romestain, H. Mariette, M. D. Sturge, N. Magnea, and H. Tuffigo, Phys. Rev. B **46**, 1557 (1992).
[37] A. Haury, diploma thesis, Universität Karlsruhe, 1995.